Analysis of UHPC Beams under Impact Loads

Serdar Astarlioglu,* (corresponding author)– Research Civil Engineer (Structural), U. S. Army Engineer Research and Development Center, Vicksburg, MS 39180 USA, Phone: (601) 634-6064, Email: Serdar.Astarlioglu@usace.army.mil

Ted Krauthammer–Professor, University of Florida, Center for Infrastructure Protection and Physical Security, 365 Weil Hall, PO Box 116580, Gainesville, FL 32611 USA, (352) 273-0690, Email: tedk@ufl.edu

Abstract:

This paper presents the results of numerical studies on the responses of normal-strength concrete (NSC) and ultra-high performance concrete (UHPC) beams subjected to impact loads using an advanced single-degree-of-freedom (SDOF) model. The constitutive models and material parameters were developed and calibrated based on the results of static and dynamic testing on NSC and UHPC cylinders at the Center for Infrastructure Protection and Physical Security (CIPPS), University of Florida. The results from the SDOF models were compared to the results obtained by static and impact testing of full-scale NSC and UHPC beams. The numerical models provided good correlation with the impact test results and were able to predict the peak response quantities with reasonable accuracy.

Permission to publish was granted by the Director, Geotechnical and Structures Laboratory. Publication is approved for public release; distribution is unlimited.

Keywords: Impact testing, SDOF, Numerical simulation

1. Introduction

The last three decades have seen the emergence of cementitious composites with compressive strengths in excess of 150 MPa. These composites, termed UHPCs, exhibit increased strength, ductility, and durability when compared to NSC. Due to such enhanced properties and performance, UHPC promises to be an ideal candidate as the material of choice in a wide range of construction projects, including protective structures.

There are several factors preventing wide-spread adoption of UHPC. First and foremost is the high cost of the material. Commercially available UHPCs, such as Ductal by LaFarge (Acker and Behloul 2004), are proprietary mixtures, and the material cost alone is more than tenfold the cost of NSC. In addition, UHPC requires much more stringent preparation and curing practices that add considerably to the cost and often prohibit use in cast-in-place-type applications. Finally, there is a big gap in the state-of-knowledge on how to analyze and design structures using this innovative material and how such structures will respond to static, dynamic, and impulsive loads. For this purpose, significant research needs to be done in order to extend the knowledge obtained, from component level (e.g., cylinder, beam, or panel) testing to guidelines and principles for structural analysis and design. A major stepping stone in achieving this goal is to develop validated and reliable constitutive models for both high-fidelity finite element-based and fast-running analysis methods.

One of the approaches for reducing the cost of UHPC is to develop nonproprietary generic mixtures that make use of locally available constituents (Allena and Newtson 2010). COR-TUF,

which was developed by the U. S. Army Engineer Research and Development Center (ERDC) for force-protection-type applications, uses traditional concrete constituent materials such as sand, cement, silica fume, and high-range water reducer; Peters 2009). In laboratory tests on cylinders and small-scale beams, COR-TUF showed material strengths comparable to commercial UHPC.

This paper details the implementation of the material models for COR-TUF with steel fibers (COR-TUF1) and without steel fibers (COR-TUF2) in the advanced fast-running computer code Dynamic Structural Analysis Suite (DSAS) (Astarlioglu and Krauthammer 2012). In the next sections, a summary of the material characteristics and experimental results obtained from these tests that were conducted on NSC, COR-TUF1, and COR-TUF2 specimens is provided, the fundamental analysis and modeling concepts adopted in DSAS are described, and the experimental results from static and impact testing of full-scale beams are compared with results of DSAS simulations.

2. Material Properties

COR-TUF is an ultra-high-performance concrete that was developed at the ERDC Geotechnical and Structures Laboratory (Roth et al. 2010; Williams et al. 2009). It is composed of fine silica sand with a maximum size of 0.6 mm, silica flour, and silica fume. COR-TUF has a very low water-to-cement ratio of 0.21, which is typical for UHPC mixes; and a high-range water reducer or "superplasticizer" is added to reduce water demand and increase the workability of the mixture during preparation. Table 1 shows the mixture proportions for COR-TUF with fibers (i.e., COR-TUF1). For comparative purposes, a COR-TUF mixture without fibers (i.e., COR-TUF2) was also prepared for this study. During the preparation, 30-mm-long, 0.55-mm-diameter steel fibers with hooked ends were added to the mix designated as COR-TUF1. The volumetric fiber content of COR-TUF1 was approximately 3.6%, which is quite high. By comparison, Ductal uses 13-mm-long, 0.2-mm-diameter straight fibers, and the amount of fibers is 2% by volume.

Table 1. Mix Proportions for COR-TUF (Williams et al. 2009)

Material	Product	Proportion by Weight
Cement	Lafarge, Class H, Joppa, MO	1
Sand	US Silica, F55, Ottawa, IL	0.967
Silica flour	US Silica, Sil-co-Sil 75, WV	0.277
Silica fume	Elkem, ES 900 W	0.389
Superplasticizer	W.R. Grace, ADVA 170	0.0171
Water (tap)	Municipal Water, Vicksburg, MS	0.208
Steel fibers (3.6%)	Bekaert, Dramix® ZP305	0.31

Material properties--including compression behavior, ultimate compressive strength, Young's modulus, and Poisson's ratio--were obtained from static cylinder testing at CIPPS. For COR-TUF1, the Young's modulus was 54.3 GPa, the Poisson's ratio was 0.20, and the

compressive strength was 199 MPa on average. For COR-TUF2, the Young's modulus was 54.5 GPa, the Poisson's ratio was 0.19, and the compressive strength was 197 MPa.

3. Numerical Analysis

In this study, the DSAS code was used to perform numerical analysis of reinforced concrete (RC) columns under blast loads. DSAS is a multifunctional dynamic analysis suite, capable of performing time-history analyses of a wide range of structural components (Astarlioglu and Krauthammer 2012; Morency et al. 2010; Tran et al. 2009). DSAS utilizes a layered section analysis approach and strain compatibility to determine the moment-curvature relationship of a structural component (i.e., a beam, a column, or a one-way slab). Then, a displacement-controlled nonlinear finite element (FE) analysis using Crisfield's cylindrical-arch length method (Crisfield 1996) is conducted to establish the resistance function and the equivalent load and mass characteristics. The resulting resistance function is then used to perform an SDOF time-history analysis of the structural component. DSAS also considers other modes of response--including direct shear, diagonal shear, and tension membrane. The direct shear analysis is performed as a failure check using the modified version of the Hawkins direct shear model (Krauthammer et al. 1986). Tension membrane and the influence of diagonal shear are incorporated into the flexural resistance function. The details of the approach used in obtaining the resistance function and conducting the time-history analysis are described below.

3.1. Resistance Function

The first step in a DSAS analysis of beams or columns is to obtain the moment versus curvature relationship for the section under consideration. This is done by dividing the section into a pre-determined number of concrete and reinforcement layers. These layers are assigned confined or unconfined concrete properties based on their location. The reinforcement layers are assigned steel properties. In all these layers, the stress-versus-strain relationship is assumed to be uniaxial. DSAS has a number of constitutive models for NSC (confined or unconfined), UHPC, and reinforcing steel. In order to perform an SDOF analysis of a structural component, one must establish the relationships that relate the continuous system, such as the one shown in **Figure 1**, to a simple mass-damper system. Furthermore, the load function under consideration should be separable into time-dependent and spatial components, where $p^t(x)$ is the load function, λ^t is the time-dependent portion of the load function, and $\bar{p}(x)$ is the spatial distribution of the load.
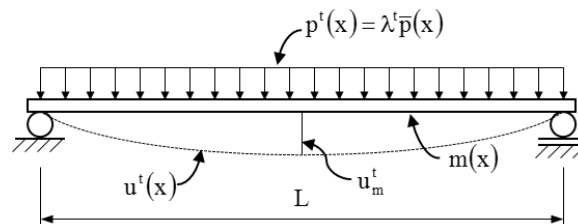
Figure 1. Structural system

The evaluation of the equivalent SDOF properties, including the resistance function, is accomplished by using a static nonlinear analysis. The reference displacement for the SDOF system is defined as the displacement of the continuous system at the point of interest (e.g., midspan) for each load increment i as shown in Eq.(1). The normalized displacement field is defined as shown in Eq.(2).

$$u_m^i = u^i \frac{L}{2} \tag{1}$$

$$\varphi^i(x) = \frac{u^i(x)}{u_m^i} \tag{2}$$

In these equations, $u^i(x)$ is the displacement field, u_m^i is the midspan displacement, and $\varphi^i(x)$ is the normalized displacement field at increment i. The equivalent load and equivalent mass for the lumped SDOF system are calculated from Eqs.(3) and (4), respectively.

$$F_e^i(x) = \int_0^L p^i(x)\varphi^i(x)dx \tag{3}$$

$$M_e^i(x) = \int_0^L m(x)\left(\varphi^i(x)\right)^2 dx \tag{4}$$

Once the static analysis is completed and the equivalent SDOF system properties are established, the Newmark-Beta method (Newmark and Rosenblueth 1972) is used to solve the dynamic equilibrium equation in Eq.(5) and to determine the component's response time history.

$$F_e^t = M_e^t \ddot{u}_m^t + C\dot{u}_m^t + R_e^t \tag{5}$$

In Eq.(5), R_e^t, M_e^t, and F_e^t are the equivalent resistance, equivalent mass, and equivalent external force at time t, respectively. $\ddot{u}_m^t, \dot{u}_m^t,$ and u_m^t are the midspan acceleration, velocity, and displacement, respectively, at time t.

3.2. Rate Effects

Under dynamic loads, the strain rate is not constant and varies across the section and along the length of the member as a function of time. Unfortunately, consideration of the time-dependent nature of strain rate in a numerical analysis may not always be practical, particularly in the context of a fast-running SDOF-based approach where all the response characteristics of a component, such as resistance and mass, are lumped. In this study, the dynamic increase factors (DIFs) for each material (e.g., concrete and steel) are calculated based on the given strain rate; and then the resulting stress-strain relationship is used for deriving the section's moment-curvature relationship and the beam's resistance function. In DSAS, the DIF for steel is determined using the following equation (Soroushian and Choi 1987):

$$DIF = \left(3.1 + 1.2f_y + \left(0.65 + 0.05f_y\right)\log_{10}\dot{\varepsilon}\right)/f_y. \tag{6}$$

For UHPC, the following equations from Ngo et al. (2007) are used.

$$DIF = \left(\frac{\dot{\varepsilon}}{\dot{\varepsilon}_s}\right)^{1.026\alpha} \qquad\qquad \dot{\varepsilon} < \dot{\varepsilon}_1$$
$$\tag{7}$$
$$DIF = A_1 \log\dot{\varepsilon} - A_2 \qquad\qquad \dot{\varepsilon} \geq \dot{\varepsilon}_1$$

where,

$$\alpha = \frac{1}{20 + f_{c,max}/2}$$

$$\dot{\varepsilon}_s = 3 \cdot 10^{-5}$$

$$\dot{\varepsilon}_1 = 0.022 \cdot f_{c,max}{}^2 - 0.1989 \cdot f_{c,max} + 46.137$$

$$A_1 = -0.0044 \cdot f_{c,max} + 0.9866$$

$$A_2 = -0.0128 \cdot f_{c,max} + 2.1396$$

3.3. Constitutive Model

Figure 2 shows the material model implemented in DSAS to represent UHPC in this study. This model is based on a compilation of stress-strain relations proposed by various researchers (Acker and Behloul 2004; Fehling et al. 2004; Habel 2004; Habel and Gauvreau 2008). The material model used to represent the reinforcing steel used in DSAS is based on the model proposed by Park and Paulay (1975) and consists of a linear elastic portion, a yield plateau, and a strain-hardening region.
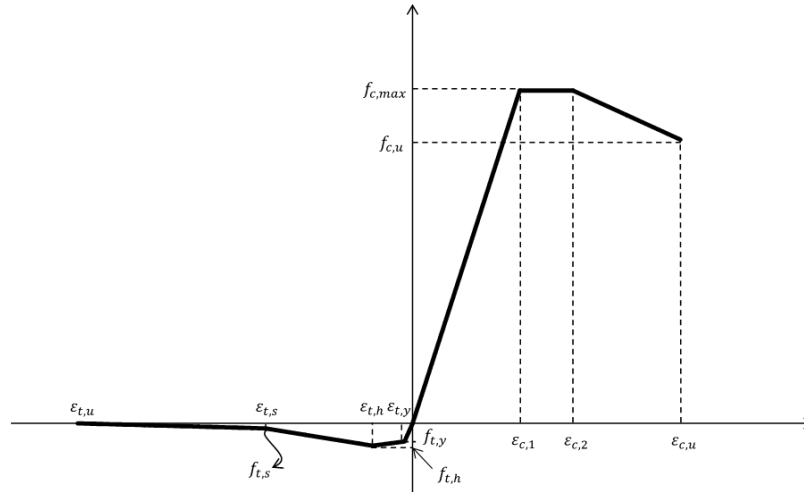
Figure 2. Stress vs. strain curve for UHPC (Acker and Behloul 2004; Fehling et al. 2004; Habel 2004; Habel and Gauvreau 2008)

4. Experimental Setup

The beams that were constructed for static and impact testing had a rectangular cross section with dimensions of 305-mm (12-in.) height, 152-mm (6-in.) width, and 3,048-mm (10-ft) length, as shown in Figure 3. These beams were cast from the same batches of concrete as the cylinders and were subjected to the same curing process to ensure that the material properties were consistent across cylinder and beam tests. Table 2 shows the designations and reinforcement details of these beams. Table 3 shows the drop number, mass and drop height for the impact tests that were compared to the numerical simulations. The NSC beams were designated as B1 and had both flexural and shear reinforcement. The COR-TUF1 beams were designated as B3 (with flexural and shear reinforcement) and B6 (with flexural reinforcement only), and the COR-TUF2 beams were designated as B4.

The clear span between the supports was 2,743 mm (108 in.), and concentrated loading was applied through a 304-mm- (12-in.-) wide stub at the center of each beam. The longitudinal reinforcement was composed of two 19.1-mm-diameter (US No 6) deformed bars at the top and two 22.2-mm-diameter (US No. 7) deformed bars at the bottom. The effective depth of the

reinforcement was 254 mm (10 in.). The tension and compression reinforcement ratios in all the beams were 2.00% and 1.47%, respectively. Shear reinforcement was provided as 9.5-mm-diameter (US No. 3) bars with a spacing of 127 mm (5 in.) on-center. The shear reinforcement ratio was 0.73 %. The design yield strength of the steel was 414 MPa (60 ksi, Grade 60). The actual yield and ultimate strengths were determined as 469 MPa (68 ksi) and 752 MPa (109 ksi), respectively, from uniaxial tensile tests conducted using samples from the same batches of steel that were in the beams.
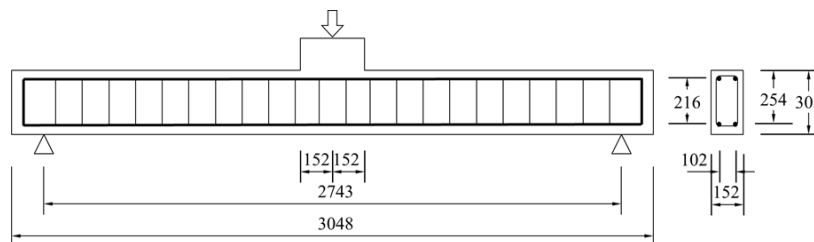
Figure 3. Test beam details (units: mm)

Table 2. Beam designations and material properties

Designation	Material	Reinforcement ratio, %		
		Tension	Compression	Shear
B1	NSC	2.00	1.47	0.73
B3	COR-TUF1	2.00	1.47	0.73
B4	COR-TUF2	2.00	1.47	0.73
B6	COR-TUF1	2.00	1.47	0.00

Table 3. Drop mass and height values for the load cases used in numerical simulations

Designation	Drop No	Drop mass, kg	Drop height, m
B1A	3	408.6	3.81
B1B	2	408.6	3.81
B1D	2	408.6	3.81
B3B	3	376.8	3.96
B3C	2	408.6	3.91
B3D	2	408.6	3.91
B3E	2	408.6	3.91
B4A	3	408.6	3.81
B4B	2	408.6	3.81
B4C	2	408.6	3.81
B4D	2	408.6	3.81
B4E	2	408.6	3.81
B6A	3	408.6	3.81
B6B	2	408.6	3.81
B6C	2	408.6	3.81
B6D	2	408.6	3.81
B6E	2	408.6	3.81

5. Results and Discussion

In this section, the midspan displacement time-histories of all the impact tests that were conducted are compared. The experimental results were plotted against the numerical results obtained from DSAS. For the B1 series tests, the peak displacements were 86, 72, and 122 mm for B1A, B1B, and B1D, respectively. The peak displacement from B1D was significantly bigger than B1A and B1B. This might have been due to manufacturing defects or any damage the specimen might have sustained during transportation. Overall, the experimental results for the NSC beams compare well with the 89-mm peak displacement reported by DSAS. The displacement vs. time histories for B1 are shown in Figure 4. The response predicted by DSAS in the post-peak phase appears to be stiffer than the experimental results. This is due to DSAS's using the initial stiffness of the beam for unloading and reloading and not accounting for any softening that occurred in the beam due to damage that occurred during the loading. This "stiffer" response was also present in the other beam types as well.

For the B3 series tests, the peak displacements for individual tests were 60, 63, and 68 mm for B3C, B3D, and B3E, respectively. The peak displacement from the DSAS simulation was 57 mm, which was smaller than all three experimental values. The difference between the average experimental peak displacement and DSAS was less than 11%. The displacement vs. time histories for B3 series are shown in Figure 5.

The B4 series beams had the same amount of longitudinal and transverse reinforcement as the B3 series beams but did not have any steel fibers. B4 series beams suffered considerable localized damage as soon as the impactor came in contact with the stub of the beam; and lots of debris, some of which were considerable in size, were ejected from the beam. In spite of the significant localized damage experienced in the B4 cases, the responses in all five tests were very consistent. The peak midspan displacements varied between 71 mm for the B4A case and 80 mm for the B4E case. The average peak midspan displacement measured in the experiments was 77 mm. The initial analysis using DSAS resulted in much smaller displacements than those observed in the experiments. In the subsequent analysis, the top cover was removed from the section to include the localized effect of the impact. The peak displacement after this modification was determined as 74 mm, which is in good agreement with the test results. The displacement time-histories for B4 are shown in Figure 6.

The B6 series beams were constructed using COR-TUF1 and had longitudinal reinforcement just like the B3 series beams. It was assumed that the steel fibers in the concrete mix would provide sufficient diagonal shear resistance, thus making any shear reinforcement in the form of stirrups redundant; and, consequently, the B6 beams were constructed without any stirrups. In these tests, the performance of the B6 beams was comparable, even favorable, to that of the B3 beams. The peak midspan displacements ranged from 54 to 64 mm in the five cases that were considered. The average peak midspan displacement from the tests was 59 mm. The displacement values predicted by DSAS fell within the range of the experimental results. The 56-mm peak displacement value predicted by DSAS was 5% lower than the average experimental displacement. The displacement time-histories for B6 are shown in Figure 7.

This paper described static and dynamic testing of full-scale NSC and UHPC beams at the Center for Infrastructure Protection and Physical Security (CIPPS), University of Florida, . The results from the experiments were compared to the numerical results from DSAS, which is a fast-running dynamic analysis software.
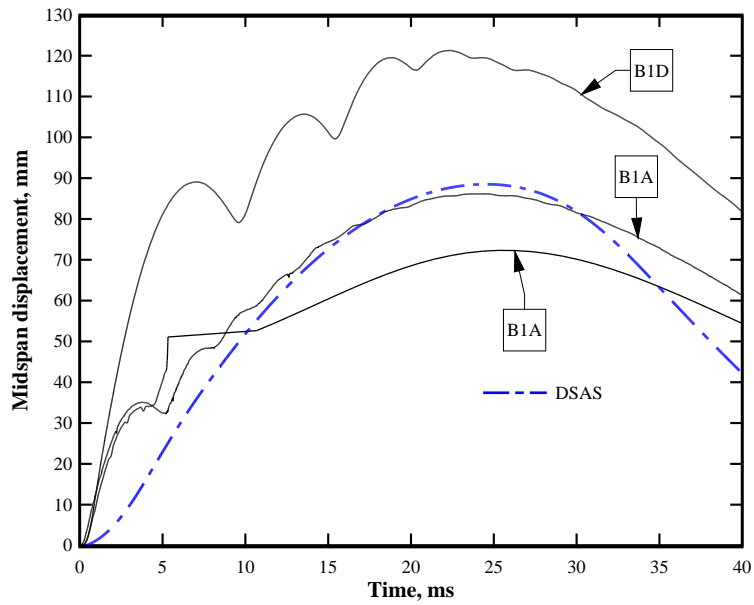
Figure 4. B1 midspan displacement time-histories
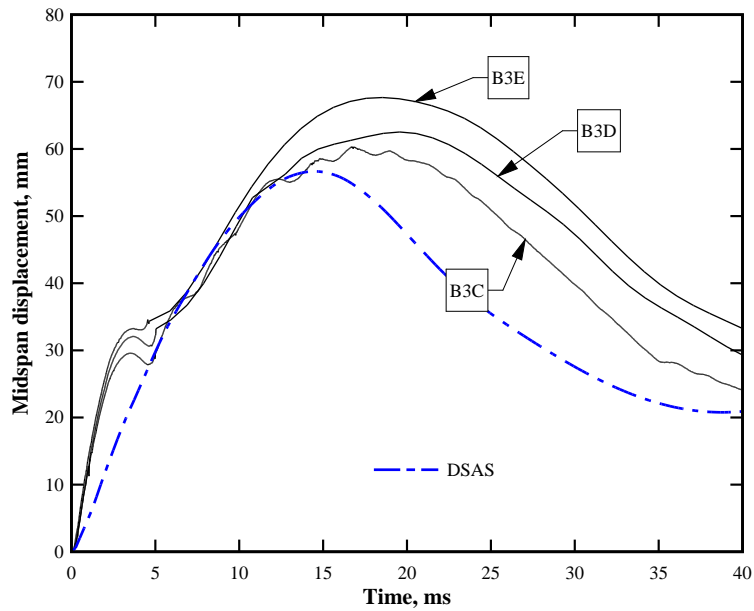
Figure 5 B3 midspan displacement time-histories
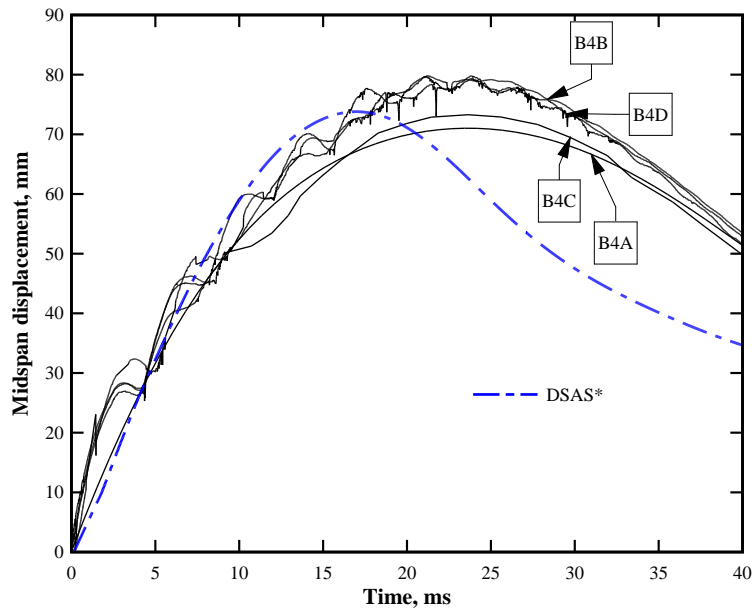
Figure 6 B4 midspan displacement time-histories
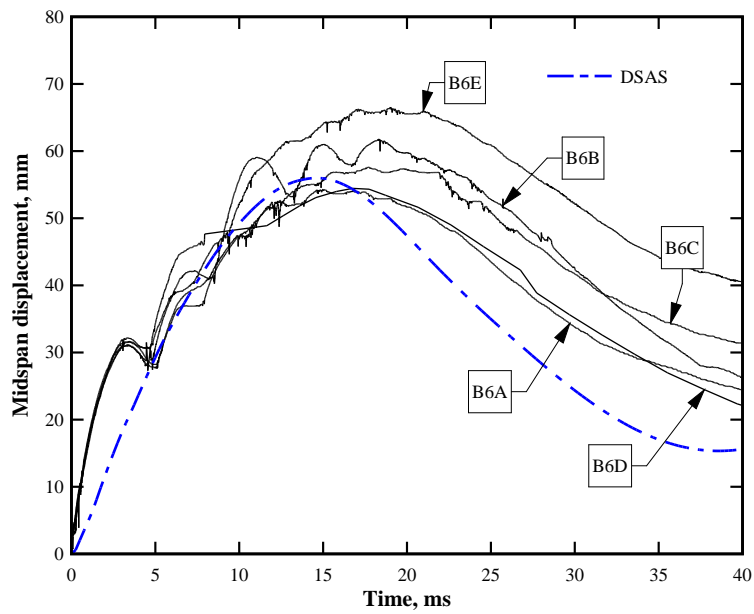
Figure 7 B6 midspan displacement time-histories

6. References

Acker, P., and Behloul, M. (2004). "Ductal technology: A large spectrum of properties, a wide range of applications." *Proceedings of the International Symposium on Ultra High Performance Concrete*, Kassel University Press, Kassel, Germany, 11–24.

Allena, S., and Newtson, C. (2010). *Ultra-high strength concrete mixtures using local materials. 2010 Concrete Sustainability Conference* , Tempe, AZ.

Astarlioglu, S., and Krauthammer, T. (2012). *Dynamic Structural Analysis Suite (DSAS) User Manual Version 4*. Center for Infrastructure Protection and Physical Security (CIPPS), University of Florida, Gainesville, FL.

Crisfield, M. A. (1996). *Non-Linear Finite Element Analysis of Solids and Structures*. Wiley, New York.

Fehling, E., Leutbecher, T., and Bunje, K. (2004). "Design relevant properties of hardened ultra high performance concrete." *International Symposium on Ultra High Performance Concrete*, Kassel, Germany, 327–338.

Habel, K. (2004). "Structural behaviour of elements combining ultra-high performance fibre reinforced concretes (UHPFRC) and reinforced concrete." Dissertation, Swiss Federal Institute of Technology, Lausanne, Switzerland.

Habel, K., and Gauvreau, P. (2008). "Response of ultra-high performance fiber reinforced concrete (UHPFRC) to impact and static loading." *Cement and Concrete Composites*, 30(10), 938–946.

Krauthammer, T., Bazeos, N., and Holmquist, T. J. (1986). "Modified SDOF analysis of RC box-type Structures." *Journal of Structural Engineering*, 112(4), 726–744.

Morency, D., Krauthammer, T., and Astarlioglu, S. (2010). *Large Deflection Behavior Effect in Reinforced Concrete Column under Severe Dynamic Short Duration Load*. Center for Infrastructure Protection and Physical Security (CIPPS), University of Florida, Gainesville, FL.

Newmark, N. M., and Rosenblueth, E. (1972). *Fundamentals of Earthquake Engineering*. Prentice Hall, Englewood Cliffs, NJ.

Ngo, T. D., Mendis, P., and Krauthammer, T. (2007). "Behavior of ultrahigh-strength prestressed concrete panels subjected to blast loading." *Journal of Structural Engineering*, 133(11), 1582–1590.

Park, R., and Paulay, T. (1975). *Reinforced Concrete Structures*. Wiley, New York.

Peters, S. J. (2009). "Fracture Toughness Investigations of Micro and Nano Cellulose Fiber Reinforced Ultra High Performance Concrete." MS Thesis, University of Maine, Orono, ME.

Roth, M. J., Rushing, T. S., Flores, O. G., Sham, D. K., and Stevens, J. W. (2010). *Laboratory Investigation of the Characterization of Cor-Tuf Flexural and Splitting Tensile Properties*. U. S. Army Engineer Research and Development Center, Vicksburg, MS, 49.

Soroushian, P., and Choi, K. (1987). "Steel mechanical properties at different strain rates." *Journal of Structural Engineering*, 113(4), 663–672.

Tran, T. P., Krauthammer, T., and Astarlioglu, S. (2009). *Effect of Short Duration High Impulse Variable Axial and Transverse Loads on Reinforced Concrete Column*. Center for Infrastructure Protection and Physical Security (CIPPS), University of Florida, Gainesville, FL.

Williams, E. M., Reed, P. A., Graham, S. S., and Rushing, T. S. (2009). *Laboratory Characterization of Cor-Tuf Concrete with and without Steel Fibers*. U. S. Army Engineer Research and Development Center, Vicksburg, MS, 83.

7. Acknowledgements (optional)